

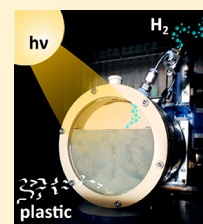
Photoreforming of Nonrecyclable Plastic Waste over a Carbon Nitride/Nickel Phosphide Catalyst

Taylor Uekert, Hatice Kasap, and Erwin Reisner*[✉]

Christian Doppler Laboratory for Sustainable SynGas Chemistry, Department of Chemistry, University of Cambridge, Lensfield Road, Cambridge CB2 1EW, U.K.

Supporting Information

ABSTRACT: With over 8 billion tons of plastic produced since 1950, polymers represent one of the most widely used—and most widely discarded—materials. Ambient-temperature photoreforming offers a simple and low-energy means for transforming plastic waste into fuel and bulk chemicals but has previously only been reported using precious-metal- or Cd-based photocatalysts. Here, an inexpensive and nontoxic carbon nitride/nickel phosphide ($\text{CN}_x/\text{Ni}_2\text{P}$) photocatalyst is utilized to successfully reform poly(ethylene terephthalate) (PET) and poly(lactic acid) (PLA) to clean H_2 fuel and a variety of organic chemicals under alkaline aqueous conditions. Ni_2P synthesized on cyanamide-functionalized carbon nitride is shown to promote efficient charge separation and catalysis, with a photostability of at least 5 days. The real-world applicability of photoreforming is further verified by generating H_2 and organics from a selection of nonrecyclable waste—including microplastics (polyester microfibers) and food-contaminated plastic—and upscaling the system from 2 to 120 mL while maintaining its efficiency for plastic conversion.



1. INTRODUCTION

The majority (86%) of plastic packaging accumulates in landfills or escapes into the environment.^{1–4} Plastic pollution represents not only a global environmental crisis but also a loss of valuable resources. Most polymers are synthesized from fossil fuels, and it is predicted that 3.5 billion barrels of oil (\$176 billion) could be saved each year if all global plastic waste were recycled.⁴ However, the implementation of widespread recycling is limited by suboptimal waste management, lack of awareness, and the diverse range of chemistries, complexities, and sizes of polymer products.^{1,2}

Small polymer pieces known as microplastics (defined as ≤ 5 mm) are particularly problematic for recycling.^{5–7} Microplastics are present in a variety of products and are also formed when plastic degrades over time.⁶ Their small size and dilution make collection and reuse challenging, which contributes to their ubiquity in oceans,^{5–7} drinking water, and salt^{8–10} around the world. Even among plastics that can be reused, recycling has its limitations. Many polymers are downcycled into lower quality products. Only 7% of recycled poly(ethylene terephthalate) (PET) bottles, for example, are recast as bottles.¹ Existing management structures are currently incapable of sustainably and economically processing the vast variety of plastic waste, and new technologies for transforming end-of-use polymers into valuable products are urgently required.

One such technology is photoreforming (PR), in which sunlight and a photocatalyst generate H_2 from an organic substrate and water. The substrate acts as an electron donor and is oxidized by the excited photocatalyst to other organic molecules. The photogenerated electrons are then transferred from the photocatalyst to a cocatalyst and reduce water to H_2 (Figure 1). H_2 is a particularly valuable product given its high

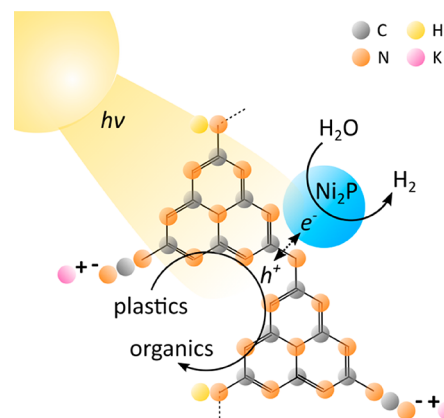


Figure 1. Schematic diagram of the polymer photoreforming process using a $\text{CN}_x/\text{Ni}_2\text{P}$ photocatalyst.

demand for agricultural, pharmaceutical, chemical, and renewable energy applications.^{11,12} Unlike existing H_2 production technologies like steam reforming of fossil fuels¹³ or thermal-based approaches for converting plastic into oil,¹⁴ PR can be conducted at ambient temperature and pressure, uses sunlight as its only energy input, and produces fuel-cell-grade H_2 .¹⁵ While photocatalytic degradation of plastics (typically to microplastics and CO_2) has been researched for several decades,^{16–18} PR offers a novel approach by not only mitigating plastic waste but also generating valuable chemical products. The thermodynamics of the overall PR process are also nearly energy neutral.¹⁹ PR of ethylene glycol at room

Received: June 28, 2019

Published: August 29, 2019

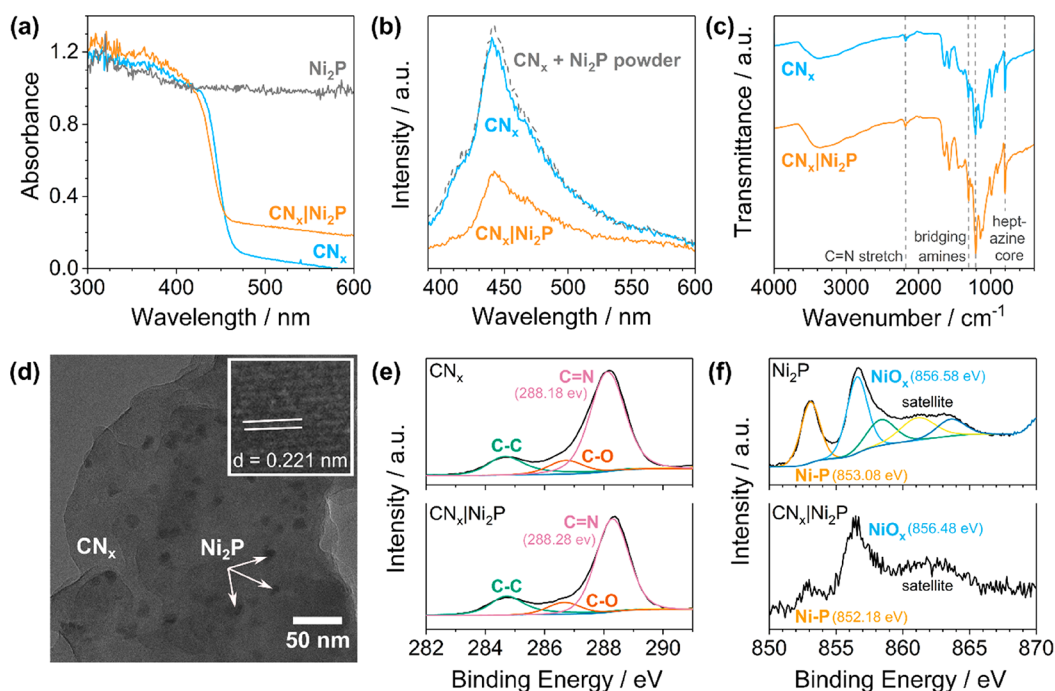


Figure 2. Characterization of the $\text{CN}_x|\text{Ni}_2\text{P}$ (2 wt %) photocatalyst. Comparison of the (a) diffuse-reflectance UV-vis, (b) emission ($\lambda_{\text{ex}} = 360$ nm, $\lambda_{\text{em}} = 450$ nm), and (c) FTIR spectra of CN_x and $\text{CN}_x|\text{Ni}_2\text{P}$. (d) TEM image of the $\text{CN}_x|\text{Ni}_2\text{P}$ catalyst, with inset showing the lattice spacing of Ni_2P . XPS spectra of the (e) C_{1s} edge for CN_x and $\text{CN}_x|\text{Ni}_2\text{P}$ and (f) Ni_{2p} edge for Ni_2P and $\text{CN}_x|\text{Ni}_2\text{P}$.

temperature requires $\Delta G^\circ = 9.2$ kJ mol $^{-1}$ ($E^\circ_{\text{cell}} = -0.01$ V, see the Supporting Information for details).

Although PR of simple molecules and biomass has been researched extensively,^{19–21} plastic substrates have been largely overlooked. The same characteristics that make polymer recycling difficult—complex structures, low water solubility, and poor biodegradability—also make PR more challenging. As a result, there are only two previous studies on PR of plastics: one employed an expensive and UV-absorbing TiO_2/Pt photocatalyst,²² whereas the other used toxic CdS/CdO_x quantum dots.²³

We propose cyanamide-functionalized carbon nitride (CN_x) coupled with a nickel phosphide (Ni_2P) H_2 evolution cocatalyst as a noble-metal- and Cd-free alternative for PR of plastic waste (Figure 1). Carbon nitride is a nontoxic and inexpensive polymeric photocatalyst,^{24–26} and the introduction of cyanamide defects improves its photocatalytic efficiency.²⁷ CN_x features a band gap of 2.7 eV that allows for visible light absorption and band edges (conduction band -0.5 V vs NHE, valence band $+2.2$ V vs NHE at pH 6)²⁸ suitable for the PR reactions. CN_x has also been used for PR of biomass with various cocatalysts under a wide pH range.²⁹ With key characteristics including visible-light absorption, alkaline stability, low cost, and nontoxicity, CN_x is a competitive alternative to both CdS/CdO_x and TiO_2/Pt for polymer PR. Ni_2P has previously been utilized with unfunctionalized carbon nitride ($^{\text{H}_2\text{N}}\text{CN}_x$) and a soluble sacrificial electron donor (triethanolamine) for H_2 evolution^{30–32} and has potential for plastic PR given its alkaline compatibility and relatively high H_2 evolution activity.³³

Here, we demonstrate that the $\text{CN}_x|\text{Ni}_2\text{P}$ photocatalyst can be employed under alkaline conditions to produce H_2 and organic chemicals from PET and poly(lactic acid) (PLA, a biodegradable but not typically recycled alternative to PET). We further apply this system to real-world, nonrecyclable

waste, including polyester microfibers and oil-contaminated PET, and show that it can be upscaled from 2 to 120 mL without efficiency losses. This proof-of-concept demonstration of noble-metal-free, Cd-free, and visible-light-driven plastic PR with $\text{CN}_x|\text{Ni}_2\text{P}$ offers a sustainable and scalable route toward simultaneous plastic waste elimination and renewable fuel and chemical synthesis.

2. SYNTHESIS AND CHARACTERIZATION OF THE PHOTOCATALYST

CN_x was prepared from melamine at 550 °C,³⁴ followed by postsynthetic functionalization with potassium thiocyanate²⁷ according to slightly modified literature procedures. $\text{CN}_x|\text{Ni}_2\text{P}$ was produced by adapting a literature synthesis:³⁰ CN_x was stirred with $\text{NiCl}_2 \cdot 6\text{H}_2\text{O}$ and $\text{NaH}_2\text{PO}_4 \cdot 2\text{H}_2\text{O}$ in H_2O , dried under vacuum, annealed at 200 °C for 1 h under Ar, washed, and dried prior to use (see the Experimental Methods section for details). Inductively coupled plasma optical emission spectrometry (ICP-OES) confirms that Ni is present in the sample at a concentration of 15.3 mg $_{\text{Ni}}$ g $_{\text{CN}_x}^{-1}$ (the ideal Ni loading of a $\text{CN}_x|\text{Ni}_2\text{P}$ -2 wt % catalyst is 15.9 mg $_{\text{Ni}}$ g $_{\text{CN}_x}^{-1}$, Table S1). However, considerably more P is observed than expected for a Ni:P ratio of 2:1 (52.2 mg $_{\text{P}}$ g $_{\text{CN}_x}^{-1}$ versus the ideal 4.2 mg $_{\text{P}}$ g $_{\text{CN}_x}^{-1}$, Table S1). This same trend is evident in the X-ray photoelectron spectroscopy (XPS) quantification results (Table S2) and can be attributed primarily to residual PO_x from the cocatalyst synthesis that adheres to the surface of CN_x (Figure S1 and Table S1) as well as to PO_x surface species on Ni_2P (Figure S2 and Table S2).^{30,35}

Diffuse-reflectance UV-vis spectroscopy shows that the $\text{CN}_x|\text{Ni}_2\text{P}$ composite retains its visible light absorption ($\lambda < 460$ nm, Figure 2a). The increased baseline at $\lambda > 460$ nm can be attributed to scattering from Ni_2P . The fluorescence emission of CN_x is quenched upon Ni_2P addition, which

could suggest reduced charge recombination due to enhanced electron transfer to the cocatalyst (Figure 2b).^{30,32} This effect stems from the close contact between CN_x and Ni₂P in the annealed photocatalyst, as Ni₂P powder mixed with CN_x does not display quenching. Fourier transform infrared (FTIR) spectroscopy confirms that the bulk properties of CN_x—characterized by vibrations at 804 cm⁻¹ (heptazine core), 1221 and 1311 cm⁻¹ (secondary amine –C–N bending), and 2177 cm⁻¹ (C=N stretch)—are unaffected by Ni₂P (Figure 2c).²⁷ Similarly, powder X-ray diffraction (XRD) patterns show only a minor shift in the CN_x lattice spacing from 3.25 to 3.30 Å upon Ni₂P addition, which is likely caused by elemental doping of the CN_x structure^{36,37} (Figure S3a). Although the cocatalyst peaks cannot be observed in XRD analysis due to the low loading (2 wt %), measurements of Ni₂P alone confirm that hexagonal Ni₂P has been successfully synthesized (Figure S3b).

Transmission electron microscopy (TEM, Figure 2d), scanning electron microscopy (SEM, Figure S4), and energy-dispersive X-ray spectroscopy (EDX, Figure S4) show that Ni₂P is uniformly distributed across CN_x. As determined from TEM, the Ni₂P nanoparticles are 9.4 ± 0.6 nm in diameter (Figure 2d and Figure S5), which is slightly smaller than Ni₂P synthesized alone (12.8 ± 1.1 nm, Figure S6). The nanoparticles also exhibit a lattice spacing of 0.22 nm, which corresponds to the (111) plane of hexagonal Ni₂P.³⁰

XPS further verifies the binding of Ni₂P to CN_x (Figure 2e,f, Figure S2, and Table S2). The high-resolution C_{1s} (Figure 2e) and N_{1s} (Figure S2a) spectra of CN_x and CN_x/Ni₂P are nearly identical, confirming that the surface properties of CN_x are largely unaffected by cocatalyst addition. Although the Ni_{2p} (Figure 2f) and P_{2p} (Figure S2b) edges of CN_x/Ni₂P are low in intensity due to the small quantity of cocatalyst (2 wt %), they still reveal similar spectra to those of bulk Ni₂P. The Ni 2p_{3/2} edge of both Ni₂P and CN_x/Ni₂P can be deconvoluted into two peaks: Ni–P and NiO_x (from surface oxidation).³⁰ Ni–P in particular shifts to a lower binding energy (from 853.08 to 852.18 eV) on CN_x. The same trend is observed in the P_{2p} spectra. These results, combined with the slight shift in the C=N peak to higher binding energies (from 288.18 to 288.28 eV in C_{1s} and from 398.58 to 398.78 eV in N_{1s}), suggest a metal–support interaction in which electron density shifts from CN_x to Ni₂P.^{27,38} This interaction should improve electron extraction and thereby enhance PR efficiency.

3. PHOTOCATALYSIS

Having established the synthesis protocol and characterization of CN_x/Ni₂P, we subsequently studied its photocatalytic performance. When compared to literature reports for ¹⁵N-CN_x/Ni₂P under the same conditions, CN_x/Ni₂P offers comparable H₂ yields with triethanolamine as a sacrificial electron donor (Table S3). We therefore applied CN_x/Ni₂P to polymer PR. All conditions—including Ni₂P loading, photocatalyst concentration, pH, and substrate treatment—were optimized for maximal total H₂ production (Figure 3a,b and Table S4).

In a typical optimized experiment, the substrate was pretreated (24 h at 40 °C with stirring in the dark) in aqueous KOH to initiate polymer breakdown and improve PR performance (Table S5).²³ Quantitative ¹H nuclear magnetic resonance (NMR) spectroscopy of the polymers shows that 72% of PLA is solubilized to lactate during pretreatment, whereas 62% of the ethylene glycol in PET is released (Table S6 and Figure S7). Terephthalate and lactate can be detected

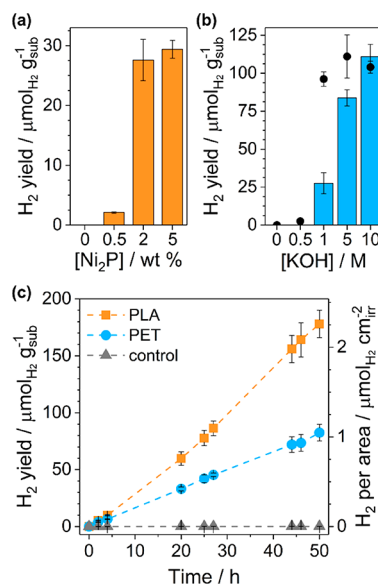


Figure 3. Photoreforming of PET and PLA with CN_x/Ni₂P. Optimization of (a) Ni₂P loading and (b) KOH concentration for photoreforming of PET (after 20 h irradiation). Black circles in (b) mark H₂ evolution per gram of substrate over CN_x/Pt (2 wt %) under the same conditions. (c) Long-term photoreforming of PET and PLA. Conditions unless stated otherwise in figure: CN_x/Ni₂P 2 wt % (1.6 mg mL⁻¹), pretreated PET (25 mg mL⁻¹), aqueous KOH (1 M, 2 mL), and simulated solar light (AM 1.5 G, 100 mW cm⁻², 25 °C).

by liquid chromatography–mass spectrometry (LC-MS analysis up to 1000 *m/z*) of the pretreated solutions of PET and PLA, respectively (Figure S8). Only a few longer chain molecules are observed, suggesting that the polymers hydrolyze primarily to their monomers.

CN_x/Ni₂P was then ultrasonicated in H₂O for 10 min following a reported procedure.²⁹ This ultrasonication process is known to increase the surface area and activity of the photocatalyst (Table S7).²⁹ The photocatalyst and pretreated substrate mixture were added to a photoreactor and exposed to simulated solar light (AM 1.5G, 100 mW cm⁻²) at 25 °C under a N₂ atmosphere. All H₂ evolution values are background-corrected by yield without substrates, which accounts for ~6% of total H₂ yield and may be at least partially due to residual P precursor from the cocatalyst synthesis (Table S8). No H₂ is detected without the photocatalyst, light absorber, cocatalyst, or light (Table S8). Mass spectrometry of the headspace gas confirms that no CO₂ is released (Figure S9a), and CO₃²⁻ is only produced from certain substrates (PLA) during PR, as determined by ¹³C NMR spectroscopy (Figure S10). Isotopic labeling experiments with D₂O verify that H₂ originates from water rather than the substrate (Figure S9b).

A Ni₂P loading of 2 wt % was optimal (Figure 3a and Table S4) as too little cocatalyst is available for electron extraction at lower loadings, whereas parasitic light absorption prevents further improvement at higher loadings.^{30–32} A variety of other noble-metal-free and alkaline-compatible cocatalysts—including Ni, Fe, and Co salts, Ni(OH)₂, Ni, Fe, and Cu oxides, and Fe_xP—were also tested with CN_x for polymer PR (Table S9). All showed inferior performance, with the second-best cocatalyst (Ni(OH)₂) offering a H₂ yield half that of Ni₂P.

Harsh conditions (e.g., high pH) are often required to solubilize plastic, and polymer PR with CN_x/Ni₂P improves

Table 1. Comparison of Photocatalysts for Photoreforming of PET and PLA^a

substrate	[base] (M)	yield ($\mu\text{mol}_{\text{H}_2} \text{g}_{\text{sub}}^{-1}$)					
		CN _x Ni ₂ P	CN _x Pt	^{H₂N} CN _x Ni ₂ P	TiO ₂ Ni ₂ P	CdS/CdO _x	TiO ₂ Pt
PET	1	33.1 ± 1.7	96.2 ± 4.8	34.3 ± 3.1	13.8 ± 2.4	132 ± 6	n.a.
	10	111 ± 8	104 ± 4	141 ± 16	119 ± 8	460 ± 58	1220 ± 110
PLA	1	59.7 ± 6.0	180 ± 17	81.2 ± 6.1	54.1 ± 9.4	56.6 ± 8.9	n.a.
	10	211 ± 10	314 ± 16	427 ± 21	220 ± 28	2910 ± 140	358 ± 53
ref		this work	this work	this work	this work	23	23

^aConditions: 25 mg mL⁻¹ pretreated PET or PLA with all catalysts except CdS/CdO_x (which used 50 mg mL⁻¹ PLA); 2 mL of aqueous KOH or NaOH solution; 1.6 mg mL⁻¹ CN_x|Ni₂P, CN_x|Pt, ^{H₂N}CN_x|Ni₂P, and TiO₂|Ni₂P; 1 nmol of CdS/CdO_x; 5 mg mL⁻¹ TiO₂|Pt; measurements taken after 20 h of simulated solar light (AM 1.5G, 100 mW cm⁻², 25 °C).

significantly with increasing pH values, from 27.6 $\mu\text{mol}_{\text{H}_2} \text{g}_{\text{sub}}^{-1}$ at 1 M KOH to 111 $\mu\text{mol}_{\text{H}_2} \text{g}_{\text{sub}}^{-1}$ at 10 M KOH (Figure 3b and Table S4). However, this enhanced H₂ yield is likely not exclusively due to improved substrate solubility, as CN_x|Pt with PET performs equally well at different molarities (black circles in Figure 3b). Instead, previous studies suggest that Ni₂P forms a thin Ni(OH)₂ layer under alkaline conditions, which is thought to improve H₂ evolution activity via enhanced water dissociation.^{30,39–41} To reduce the cost and corrosiveness of the system, all following experiments were conducted in 1 M KOH.

A variety of common polymers—polyethylene, PET, PLA, polypropylene, polystyrene, polyurethane, and polystyrene-*block*-polybutadiene (rubber)—were photoreformed under these optimized conditions (Table S10). While all polymers produced small quantities of H₂, PET and PLA offered the highest yields and were selected for further study. Both PET and PLA are polar polymers and contain esters, which facilitates hydrolysis in alkaline aqueous media and could account for their superior performance.

After 50 h of irradiation, 82.5 ± 7.3 and 178 ± 12 $\mu\text{mol}_{\text{H}_2} \text{g}_{\text{sub}}^{-1}$ were produced from PET and PLA, respectively (Figure 3c and Table S11). The values correspond to turnover numbers of 7.8 ± 0.7 and 16.8 ± 1.1 mol_{H₂} mol_{Ni}⁻¹ for the respective polymers as well as external quantum yields at $\lambda = 430 \text{ nm}$ of 0.035 ± 0.005% for PET and 0.101 ± 0.018% for PLA (Table S12). H₂ conversions—defined as the moles of H₂ detected divided by the theoretical H₂ yield—of 4.4 ± 0.6% and 1.6 ± 0.2% were achieved after 8 days of PR with PET and PLA, respectively (Table S13). Note that these calculations assume that only the aliphatic portion of PET is oxidized during PR, as is consistent with previous reports.²³ The system was still active after 8 days, suggesting that higher H₂ conversions could be achieved at longer time scales (for example, H₂ conversions of 50% are observed after 18 days of ethylene glycol PR, Figure S11). At higher pH (10 M KOH), H₂ conversions increase to 24.5 ± 3.3% for PET and 6.7 ± 0.8% for PLA (Table S13). Values reported for CdS/CdO_x under the same conditions were 16.6 ± 1.0% for PET and 38.8 ± 4.0% for PLA.²³ CN_x|Ni₂P also maintains 17% of its efficiency under visible-light-only irradiation ($\lambda > 420 \text{ nm}$, Table S8), showcasing its improved absorption range over both TiO₂ (0% retention) and ^{H₂N}CN_x (2–9% retention, Figure S12 and Table S14).

The H₂ yield from PET over CN_x|Ni₂P is 4 times lower than that with CdS/CdO_x (Table 1 and Table S15). CN_x|Ni₂P requires an electron transfer process from the light absorber to cocatalyst, which likely limits its photocatalytic efficiency in

comparison to CdS/CdO_x. For further comparison, CN_x|Pt, ^{H₂N}CN_x|Ni₂P, and TiO₂|Ni₂P were prepared and studied under identical conditions (Table 1 and Table S14). As expected, the benchmark Pt catalyst improves H₂ yield by 3 times. After 20 h of PR, ^{H₂N}CN_x|Ni₂P offers H₂ yields similar to (or in some cases higher than) CN_x|Ni₂P. This indicates the applicability of Ni₂P to a range of carbon nitrides. However, the activity of ^{H₂N}CN_x|Ni₂P decreases over time, whereas that of CN_x|Ni₂P remains constant (Figure S13 and Table S14). Future investigations will determine the reasons behind this variation, but CN_x was selected for the current work due to its apparent high long-term stability and superior utilization of visible light. Finally, TiO₂|Ni₂P has lower yields at 1 M KOH and only absorbs ultraviolet light (no H₂ observed at $\lambda > 420 \text{ nm}$, Table S14). PR of lactic acid (the monomer of PLA) is also faster on CN_x|Ni₂P (1.55 ± 0.19 $\mu\text{mol}_{\text{H}_2} \text{g}_{\text{sub}}^{-1} \text{h}^{-1}$, Table S16) than a reported ^{H₂N}CN_x|WS₂ system in H₂O (0.50 $\mu\text{mol}_{\text{H}_2} \text{g}_{\text{sub}}^{-1} \text{h}^{-1}$).⁴² CN_x|Ni₂P is thus characterized by unique benefits including low expense, visible light absorption, and long-term stability, all of which are critical parameters for scalable PR of plastics.

4. POSTCATALYSIS CHARACTERIZATION

Characterization of the CN_x|Ni₂P catalyst after PR of PLA by TEM (Figure S14), SEM/EDX (Figure S4), and XPS (Figure S15 and Table S2) confirms that Ni remains on the CN_x surface. ICP-OES shows a loading of 15.1 mg_{Ni} g_{CN_x}⁻¹ and that leaching into the PR solution is minimal (0.9% of the original Ni content). The P content decreases significantly to 8.8 mg_P g_{CN_x}⁻¹ presumably due to the loss of surface PO_x species (as observed in XPS, Figure S15). The absorption of the photocatalyst increases in the visible range after use (Figure S14), potentially due to agglomeration (Figure S4), but emission remains constant before and after PR (Figure S14). FTIR spectroscopy shows that the NCN functionality of CN_x remains intact (Figure S14), and XPS confirms that the surface properties of CN_x are unchanged after catalysis (no shifts in the C_{1s} and N_{1s} edges detected, Figure S15). XPS also shows that the Ni–P and NiO_x species in the Ni_{2p} spectrum are replaced by Ni(OH)₂ at 855.98 eV (Figure S15), which is consistent with the literature^{30,39,40} and results mentioned in the previous section. Because of its insolubility, the catalyst can be easily separated from solution by centrifugation and reused while maintaining half of its original photocatalytic activity (Table S17). This loss of activity can likely be attributed to agglomeration during the isolation/drying process or minor chemical changes in the CN_x structure, rather than to an intrinsic photocatalytic instability. When CN_x|Ni₂P is left in

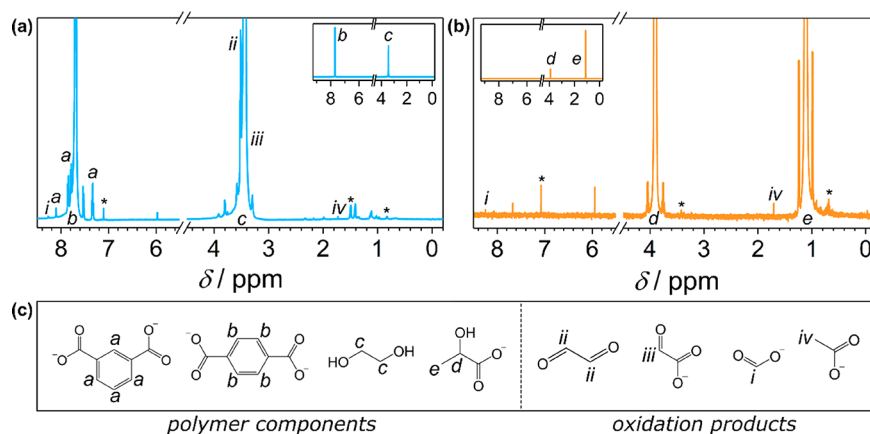


Figure 4. ^1H NMR spectra of (a) PET and (b) PLA after photoreforming. Insets show zoomed-out views of the spectra. (c) Chemical structures and peak assignments. Peaks labeled with an asterisk (*) are seen in a control sample with no substrate. Photoreforming conditions: $\text{CN}_x\text{Ni}_2\text{P}$ 2 wt % (1.6 mg mL^{-1}), pretreated polymer (25 mg mL^{-1}), NaOD (1 M) in D_2O (2 mL), simulated solar light (5 days, AM 1.5G, 100 mW cm^{-2} , 25°C).

solution, it remains active over 18 days of ethylene glycol PR until all substrate is consumed (Figure S11).

5. SUBSTRATE OXIDATION

Ideally, PR would generate useful products not only during the reduction half-reaction (H_2) but also through polymer oxidation. Although CO_2 is the expected final oxidation product, gaseous CO_2 was not detected and CO_3^{2-} was only evident after PR of PLA (Figures S9 and S10). We therefore used ^1H NMR spectroscopy to analyze the reaction mixtures and identify organic oxidation products. All peak assignments were verified by adding authentic samples (Figure S16), and maleic acid was used as a standard.

The ^1H NMR spectra show that both PET and PLA form a variety of oxidation products after 5 days of PR (Figure 4, Figure S10, and Table 2). During pretreatment under alkaline

Table 2. Quantification of the Organic Oxidation Products Formed from PET and PLA after 5 days of Photoreforming^a

	organic compound	quantity (nmol)
photoreforming of PET	acetate	190
	formate	190
	glycolate	n.a.
	glyoxal	9300
photoreforming of PLA	acetate	100
	formate	95

^aMaleic acid was used as a reference standard. Glycolate was not quantifiable as its peak overlaps with that of ethylene glycol (n.a. indicates not available).

conditions, PET hydrolyzes to its monomers—terephthalate (TPA, *b*) and ethylene glycol (EG, *c*, also see Figures S7 and S8)—or soluble oligomer fragments. TPA is not oxidized during PR (no H_2 produced, Table S16, and no oxidation products observed, Figure S17), as aromatic moieties are challenging to photoreform.²³ Because of its insolubility under most aqueous conditions, TPA could potentially be isolated and reused for PET synthesis. Isophthalate (*a*), an isomer of TPA, is present in small quantities in the original polymer and is not an oxidation product.

The EG portion of PET is oxidized by $\text{CN}_x\text{Ni}_2\text{P}$ to formate (*i*), glyoxal (*ii*), glycolate (*iii*), acetate (*iv*), and other intermediates (unlabeled). Glyoxylate and glycoaldehyde cannot be unambiguously detected in the ^1H NMR spectrum due to their overlap with the D_2O and EG peaks, respectively, but become visible in the ^{13}C NMR spectrum (Figure S10a, labeled as *v* and *vi*). Signals marked with an asterisk (*) are already present in a control spectrum of $\text{CN}_x\text{Ni}_2\text{P}$ irradiated without a polymer substrate and can be attributed to residual solvents from the photocatalyst synthesis or other impurities. PR of EG alone offers high H_2 evolution activities ($46 \pm 6 \mu\text{mol}_{\text{H}_2} \text{ g}_{\text{cat}}^{-1} \text{ h}^{-1}$, Table S16) and generates the same array of oxidation products (Figure S17).

With the exception of acetate, all of these oxidation products can be formed according to the proposed mechanism in Figure S18a. In brief, ethylene glycol is expected to oxidize to glycoaldehyde, followed by glyoxal and glycolate, glyoxylate, oxalate, formate, and finally CO_3^{2-} . PR of the oxidation products followed by ^1H NMR analysis at various time intervals (Figure S17, Tables S16 and S18) also supports the proposed series of reactions. However, the use of highly alkaline conditions during PR initiates a variety of other reactions, such as aldol condensation. These processes add further complexity and likely explain the appearance of acetate and other unidentified products corresponding to the unlabeled peaks in the ^1H and ^{13}C NMR spectra. None of the more oxidized intermediates—formate, acetate, and CO_3^{2-} —seem to accumulate over extended PR time scales (Figure S11). This leads to a mass imbalance between the quantity of measurable oxidation products and H_2 , which can likely be attributed to the additional unidentified chemicals observed in ^{13}C NMR spectroscopy (Figure S10a).

PLA offers a much simpler system. It hydrolyzes to lactate (*d*, *e*, also see Figures S7 and S8) during pretreatment, which is then oxidized primarily to CO_3^{2-} and small quantities of formate (*i*), acetate (*iv*), and other unidentified products (Figure 4b, Figures S10b and S18b). All of the above results are similar to those reported for PR of PET with CdS/CdO ²³ as well as for the oxidation of EG^{43–45} and lactate^{46,47} under a variety of conditions. The acidic products also slightly reduce the pH of the PR system, from 14.0 to 13.2 after 5 days.

Although the accumulation of organic products causes incomplete conversion of the plastic precursors to H_2 , it also

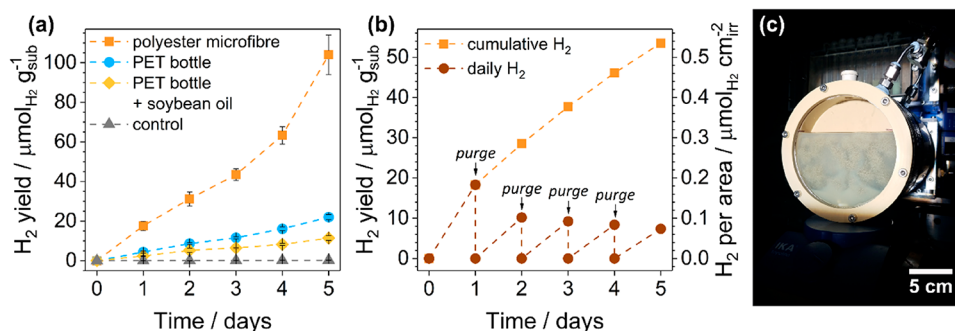


Figure 5. Photoreforming of nonrecyclable plastic waste. (a) Long-term photoreforming of polyester microfibers, a PET bottle, and an oil-coated PET bottle. (b) Upscaled photoreforming of polyester microfibers; sample was purged every 24 h. Conditions: CN_x/Ni₂P (1.6 mg mL⁻¹), 1 M KOH (2 mL for part a and 120 mL for part b), pretreated microfibers (5 mg mL⁻¹) or PET bottle (25 mg mL⁻¹) without or with soybean oil (5 mg mL⁻¹), simulated solar light (AM 1.5G, 100 mW cm⁻²). (c) Photograph of the batch reactor in use.

prevents the release of greenhouse gases like CO₂ and potentially allows for the extraction of additional chemicals. In the future, this system could be improved by tailoring the selectivity of the oxidation half-reaction toward a single high-value product. For example, acetate had a global market of 13 million tons in 2015 and is widely used as a platform chemical.⁴⁸ The development of selective oxidation cocatalysts remains a key challenge for polymer PR.

PR is often believed to proceed via hydroxyl (OH[•]) radicals.^{19,49} To investigate this possibility, we performed PR with the OH[•] scavenger TPA. TPA reacts with OH[•] to form 2-hydroxyterephthalic acid (TPA-OH), which fluoresces at λ = 430 nm when excited at λ = 315 nm. After 20 h of PR, no TPA-OH emission was detected (Figure S19). This, combined with a previous proposal that holes photogenerated on CN_x are not oxidizing enough to produce OH[•],^{29,50} suggests that OH[•] plays a minimal role in PR. Instead, PR likely proceeds via direct hole transfer between CN_x and the substrate.

6. APPLICATION TO REAL-WORLD WASTE AND MICROPLASTICS

Finally, we evaluated the real-world efficacy of the CN_x/Ni₂P system through long-term PR of polyester microfibers and food-contaminated PET (Figure 5a). Polyester microfibers are known to shed from synthetic clothing and enter the environment and drinking water.^{8,51} Despite their prevalence, their dilution and aquatic state make microplastics challenging to reuse. Another common recycling issue is food contamination, which congests equipment and reduces the quality of recovered plastic.⁵² PR could therefore be an ideal vehicle for transforming these nonrecyclable plastic items into valuable products.

The lowest possible microfiber loading was utilized (5 mg mL⁻¹; no H₂ was detected at lower loadings after 20 h, Table S19) to approach real-world conditions. Note that this concentration is still much higher than that seen in European tap water: 3.8 fibers L⁻¹.⁸ In addition, a commercial PET bottle was ground into pieces ≤0.5 cm² and coated with soybean oil (25 mg mL⁻¹ bottle, 5 mg mL⁻¹ oil). All other parameters—including catalyst concentration, pH, and pretreatment—were kept consistent with PR of pure polymers.

After 5 days of illumination, yields of 104 ± 10, 22.0 ± 1.3, and 11.4 ± 1.2 μmol_{H₂} g_{sub}⁻¹ were achieved from microfibers, a PET bottle, and oil-contaminated PET, respectively (Figure 5a and Table S20). The PR rate with microfibers increases over

time as more surface area is exposed for hydrolysis; SEM shows that the sample develops cracks and pits after PR (Figure S20). Note that the H₂ yield of microfibers is higher than that of the PET bottle because of the quantity of substrate utilized; the activities of the microfibers and PET bottle are equivalent (2.67 ± 0.25 and 2.87 ± 0.16 μmol_{H₂} g_{cat}⁻¹ h⁻¹, respectively). Oil limits access to the PET bottle, accounting for its lower performance in comparison to the bottle alone. These samples offer PR rates one-tenth that of pure PET, likely due to additional fillers and lower solubility (only 25% of the ethylene glycol in the microfibers was released after pretreatment in comparison to 62% from pure PET; Figure S7 and Table S6). ¹H NMR spectroscopy of the PR solutions after catalysis shows that the polyester microfibers oxidize primarily to glyoxal (2440 nmol after 24 h) and acetate (2100 nmol, Figure S21). The PET bottle, meanwhile, yields a wide range of oxidation products similar to those observed in pure PET (Figure S21). This provides an initial demonstration of the transformation of real-world plastic waste into both H₂ and organics.

7. UPSCALING OF PHOTOREFORMING

Compatibility with upscaling is essential for any technology aimed at eliminating global plastic waste. Having demonstrated small-scale PR of nonrecyclable plastic waste, we therefore upscaled our setup from 2 to 120 mL (Figure 5b,c and Table S20). With an irradiation area of 60 cm² and depth of 2 cm, the reactor was semioptimized for maximal light absorption. All concentrations (catalyst, substrate, and KOH) were kept constant. With this new setup, 53.5 μmol_{H₂} g_{sub}⁻¹ was generated from PR of microfibers over the course of 5 days. In contrast to small-scale PR of microfibers, the upscaled H₂ production rate decreases gradually over time. This is likely due to inefficient stirring in the reactor rather than catalyst degradation (as we have shown that CN_x/Ni₂P is stable under PR conditions). When adjusted for area of irradiation, the upscaled H₂ production (0.53 μmol_{H₂} cm⁻²) is greater than that achieved at small scales (0.26 ± 0.03 μmol_{H₂} cm⁻²), which is a promising support for the scalability of PR. However, it should be noted that the quantity of H₂ generated is equivalent to 17.9 μWh (0.00215 Wh), meaning that a 15 m² reactor would be required to charge a typical smartphone (5 Wh)⁵³ with the modest quantum yield currently offered by CN_x/Ni₂P.

As these numbers suggest, polymer PR cannot currently compete with either established H₂ production technologies (steam reforming of fossil fuels, ~80–90% conversion)¹³ or gasification of plastic to H₂ (~65–95% conversion and plastic consumption rates in the order of kg h⁻¹, depending on the specific technology).⁵⁴ To enhance the real-world applicability of plastic PR, future work must focus on key bottlenecks including catalyst efficacy, conversion rates and selectivity, substrate solubilization, reduction or reuse of KOH, and reactor design.

8. CONCLUSION

In this work, we have established a noble-metal- and Cd-free photocatalyst for visible-light-driven reforming of plastic waste. CN_x/Ni₂P functions due to the strong binding of the Ni₂P cocatalyst to CN_x, which promotes charge separation, catalytic efficiency, and stability. The CN_x/Ni₂P photoreforming system successfully generates H₂ by using PET and PLA as abundant and freely available waste feedstocks. The oxidation half-reaction is suggested to proceed via direct hole transfer from the photocatalyst to the substrate and yields valuable organic chemicals (e.g., acetate and formate) rather than CO₂, thereby improving the sustainability and overall process value of the system. CN_x/Ni₂P can also reform real-world polymer samples, including polyester microfibers and oil-contaminated PET, at both small (2 mL) and larger (120 mL) scales. These results showcase a unique benefit of photoreforming: its applicability to waste materials that cannot otherwise be recycled or reused. Plastic is a valuable resource that contains stored energy and chemical feedstocks, yet much of its potential is lost to landfills and environmental pollution. Polymer photoreforming with CN_x/Ni₂P takes advantage of this underutilized resource to simultaneously reduce plastic pollution and generate H₂ and organics in an inexpensive, sustainable, and sunlight-driven process.

9. EXPERIMENTAL METHODS

Reagents. Chloroplatinic acid (8 wt %), ethylene glycol, L-(+)-lactic acid, melamine, polypropylene, polystyrene (pellets, *M_w* 35000), and polystyrene-*block*-polybutadiene were purchased from Sigma-Aldrich. Low-density polyethylene (powder, 300 μm), poly(ethylene terephthalate) (powder, 300 μm), poly(lactic acid) (pellets, 3 mm), and polyurethane (foam, 10 × 100 × 100 mm³, density 0.08 g cm⁻³) were obtained from Goodfellow Cambridge Ltd. Polypropylene, polystyrene, polystyrene-*block*-polybutadiene, poly(lactic acid), and polyurethane were frozen with liquid N₂ and then ground in a coffee grinder to powders prior to use. NaOD (40 wt % in D₂O), KOH (semiconductor grade), KSCN, maleic acid, nickel(II) chloride hexahydrate, sodium hypophosphite monohydrate, soybean oil, and terephthalic acid were purchased from Fischer Scientific. D₂O (99.96 atom % D) was obtained from Euriso-Top, and TiO₂ nanoparticles (P25, 10–30 nm) were purchased from SkySpring Nanomaterials, Inc. A plastic water bottle (still Scottish mountain water) was purchased from Marks and Spencer Simply Food, dried, and ground by using a coffee grinder into pieces ≤0.5 cm². Polyester microfibers (Homescares Super Microfibre) were used as received.

Synthesis of Carbon Nitride. Unfunctionalized carbon nitride (H₂N₂CN_x) was prepared by heating melamine to 550 °C for 3 h under air according to a modified literature procedure.³⁴ The obtained powder was ground with a pestle and mortar. Cyanamide-functionalized carbon nitride (CN_x) was prepared by combining H₂N₂CN_x and KSCN (weight ratio 1:2) and heating first to 400 °C for 1 h followed by 500 °C for 30 min (ramp rate 30 °C min⁻¹) under Ar.²⁷ After cooling naturally, the powder was washed with H₂O and dried under vacuum at 60 °C.

Synthesis of Ni₂P. NiCl₂·6H₂O and NaH₂PO₂·H₂O (ratio of 1:5) in a minimum amount of water were first stirred for 1 h and then sonicated for 1 h. The mixture was dried under vacuum at 60 °C. The dry solid was then heated for 1 h at 200 °C under Ar (ramp rate 5 °C min⁻¹). After cooling to room temperature, the black powder was washed with water (2×) and ethanol (1×) and dried under vacuum at 60 °C.

Synthesis of Ni₂P with Light Absorber. Analogous to a previously reported procedure,³⁰ CN_x/H₂N₂CN_x or TiO₂ nanoparticles (300 mg) and NiCl₂·6H₂O (20 mg for 2 wt %) were combined in a minimum of water (1 mL), stirred first for 1 h, and then sonicated for 1 h. NaH₂PO₂·H₂O (100 mg for 2 wt %) was subsequently added to the Ni mixture and again stirred and sonicated for 1 h each. The mixture was dried under vacuum at 60 °C. The dry solid was heated for 1 h at 200 °C under Ar (ramp rate 5 °C min⁻¹). After cooling to room temperature, the powder was washed with water (3×) and ethanol (3×) and dried under vacuum at 60 °C.

Physical Characterization. Emission spectra (λ_{ex} = 360 nm, λ_{em} = 450 nm) were recorded on an Edinburgh Instruments F55 spectrofluorometer equipped with a Xe lamp and integrating sphere. All samples were prepared at a concentration of 1.6 mg mL⁻¹ in 1 M aqueous KOH in a quartz glass cuvette (1 cm path length). UV–vis spectra were recorded on a Varian Cary 50 UV–vis spectrophotometer using a diffuse reflectance accessory. Fourier transform infrared spectroscopy (FTIR) spectra were collected on a Thermo Scientific Nicolet iS50 FTIR spectrometer (ATR mode). Powder X-ray diffraction (XRD) was conducted on a PANalytical Empyrean Series 2 instrument using Cu Kα irradiation. Scanning electron microscopy (SEM) and energy dispersive X-ray spectroscopy (EDX) were conducted on a TESCAN MIRA3 FEG-SEM. Samples were sputter-coated with a 10 nm layer of either Pt or Cr prior to microscopy. Transmission electron microscopy (TEM) was conducted on a Thermo Scientific (FEI) Talos F200X G2 TEM. All samples were dispersed in ethanol at low concentrations (~4 μg mL⁻¹) and drop-cast on carbon-coated Cu grids.

Samples for X-ray photoelectron spectroscopy (XPS) were dispersed in ethanol (concentration of 5 mg mL⁻¹) and drop-cast (50 μL, 7×) onto clean FTO glass slides and dried. XPS was performed on a Thermo Fisher Scientific K-alpha⁺ spectrometer. Samples were analyzed using a microfocused monochromatic Al X-ray source (72 W) over an area of ~400 μm. Data were recorded at pass energies of 150 eV for survey scans and 40 eV for high-resolution scans with 1 and 0.1 eV step sizes, respectively. Charge neutralization of the sample was achieved through a combination of both low-energy electrons and argon ions. Three well-separated areas were selected on each sample for analysis to examine any surface heterogeneity. Data analysis was performed in CasaXPS using a Shirley type background and Scofield cross sections, with an energy dependence of -0.6.

Inductively coupled plasma optical emission spectrometry (ICP-OES) measurements were completed by the Microanalysis Service at the University of Cambridge (Department of Chemistry) on a Thermo Scientific iCAP 700 spectrometer. For quantification of the bulk Ni and P content of the catalyst before and after PR, the catalyst was digested in 2:1 H₂O₂:H₂SO₄ overnight before measurement.

Nuclear Magnetic Resonance (NMR) Spectroscopy. ¹H NMR and ¹³C NMR spectra were collected on either a 400 or 500 MHz Bruker spectrometer. All samples, including polymers before and after PR and pure oxidation intermediates and products, were prepared in 1 M NaOD in D₂O with sample concentrations of 25 mg mL⁻¹.

Quantitative ¹H NMR Spectroscopy. Samples (typically 150 μL) were spiked with a known quantity (typically 20–40 μL) of a standard solution (50 mg mL⁻¹ maleic acid in D₂O) after pretreatment or PR, depending on the experiment. The quantity of analyte (*m_{analyte}*) in the sample was calculated via eq 1:

$$m_{\text{analyte}} = \frac{I_{\text{analyte}}}{I_{\text{standard}}} \frac{N_{\text{standard}}}{N_{\text{analyte}}} \frac{M_{\text{analyte}}}{M_{\text{standard}}} m_{\text{standard}} \quad (1)$$

where *I_{analyte}* is the integral of the analyte peak, *N_{analyte}* the number of protons corresponding to the analyte peak, *M_{analyte}* the molar mass of

the analyte, and m_{standard} the known mass of the standard in the sample.

pH Measurements. pH was measured on a Mettler Toledo pH meter and probe. Samples in 1 M KOH were diluted to 0.1 M KOH prior to measuring to avoid damaging the probe, and the pH was back-calculated by using the assumption that $a[\text{OH}^-] \approx c[\text{KOH}]$.

Substrate Pretreatment. Following a slightly modified reported procedure,²³ polymers (50 mg mL⁻¹) were soaked in 2 M aqueous semiconductor-grade KOH in a sealed vial for 24 h at 40 °C with stirring at 300 rpm. The solution—including the undissolved pieces of polymer—was then used for PR as below.

Light Chromatography–Mass Spectrometry (LC-MS). Ten microliters of pretreated solution was added to 1 mL of methanol and submitted for analysis to the mass spectrometry team at the University of Cambridge (Department of Chemistry) on a ThermoFinnigan Orbitrap setup combined with a Dionex Ultimate 3000 HPLC.

Photocatalytic Generation of H₂. A dispersion of the catalyst (CN_x/Ni₂P, ¹⁵N/CN_x/Ni₂P, or TiO₂/Ni₂P) in H₂O (5 mg mL⁻¹) was ultrasonicated as described previously (10 min, pulses of 30 s at 100% amplitude followed by 5 s pauses).²⁹ The resulting mixture (0.65 mL), 1 mL of pretreated polymer in 2 M aqueous semiconductor-grade KOH, and 0.35 mL of H₂O were used per sample. Final conditions were 2 mL of 1 M aqueous KOH, 1.6 mg mL⁻¹ catalyst, 25 mg mL⁻¹ polymer, or PET bottle (5 mg mL⁻¹ used for polyester microfibers). CN_x/Pt was made by ultrasonating CN_x and then adding H₂PtCl₆ as a precursor (Pt forms via in situ photodeposition). The prepared samples were added to Pyrex glass photoreactor vials (internal volume 7.91 mL) and capped with rubber septa. After briefly vortexing, the samples were purged with N₂ (containing 2% CH₄ for gas chromatographic analysis; no CH₄ was observed in the samples postillumination without the addition of this internal standard) at ambient pressure for 10 min. The samples were then irradiated by a solar light simulator (Newport Oriel, 100 mW cm⁻²) equipped with an air mass 1.5 global (AM 1.5G) filter and a water filter to remove infrared radiation. Visible-light-only experiments were conducted by adding a $\lambda > 420$ nm cutoff filter. All samples were stirred at 600 rpm and kept at a constant temperature of 25 °C during irradiation. H₂ generation was monitored by periodically analyzing samples of the reactor head space gas (50 μ L) by gas chromatography (see below). Overpressure within the vial is minimal (an increase of 0.03 atm per 10 μ mol of H₂ produced).

Gas Analysis. The accumulation of H₂ was measured via gas chromatography on an Agilent 7890A gas chromatograph equipped with a thermal conductivity detector and HP-5 molecular sieve column using N₂ as the carrier gas. Methane (2% CH₄ in N₂) was used as an internal standard after calibration with different mixtures of known amounts of H₂/N₂/CH₄. CO₂ detection was performed with mass spectrometry on a Hiden Analytical HPR-20 benchtop gas analysis system fitted with a custom-designed 8-way microflow capillary inlet to a HAL 101 RC electron impact quadrupole mass spectrometer with a Faraday detector.

Upscaled Photocatalytic Generation of H₂. CN_x/Ni₂P (170 mg) in H₂O (15 mL) was ultrasonicated as described above and added to a photoreactor. The utilized photoreactor (internal volume 190 mL) is constructed from PEEK and stainless steel and features a quartz window (11 cm diameter). 60 mL of pretreated polyester microfibers (600 mg) in 2 M aqueous KOH and 45 mL of H₂O were also added to the photoreactor. The final experimental conditions were the following: 120 mL of 1 M aqueous KOH, 1.42 mg mL⁻¹ CN_x/Ni₂P, and 5 mg mL⁻¹ microfibers. The reactor was capped with a rubber septum and purged with N₂ (containing 2% CH₄ for gas chromatographic analysis) for 30 min. The sample was then irradiated at room temperature by a solar light simulator (LOT-Quantum Design, 100 mW cm⁻²) equipped with an air mass 1.5 global filter (AM 1.5G).

Treatment of Data. All analytical measurements were performed in triplicate, unless otherwise stated, and are given as the unweighted mean \pm standard deviation (σ). All measurements are listed as H₂

yield per weight of substrate ($\mu\text{mol}_{\text{H}_2} \text{g}_{\text{sub}}^{-1}$) and activity per weight of catalyst ($\mu\text{mol}_{\text{H}_2} \text{g}_{\text{cat}}^{-1} \text{h}^{-1}$). σ was calculated via eq 2:

$$\sigma = \sqrt{\frac{\sum (x - \bar{x})^2}{n - 1}} \quad (2)$$

where n is the number of repeated measurements, x the value of a single measurement, and \bar{x} the unweighted mean of the measurements. σ was increased to 5% of \bar{x} in the event that the calculated σ was below this threshold.

External Quantum Yield (EQY) Determination. Ultrasonicated CN_x/Ni₂P 2 wt % (3.2 mg), pretreated polymer (50 mg), and 1 M aqueous KOH (2 mL) were added to a quartz cuvette (path length 1 cm), which was then sealed with a rubber septum. The sample was purged with N₂ containing 2% CH₄ for 10 min. The sample was next activated via 4 h of illumination in a solar light simulator (Newport Oriel, 100 mW cm⁻²) equipped with an air mass 1.5 global filter (AM 1.5G) and a water filter to remove infrared radiation. After a second round of N₂ purging, the sample was irradiated by a Xe lamp (LOT LSH302) fitted with a monochromator (LOT MSH300) focused at a single wavelength of $\lambda = 430$ nm (accurate to a full width at half-maximum of 5 nm). The light intensity was adjusted to $\sim 1000 \mu\text{W cm}^{-2}$, as measured with a power meter (ILT 1400, International Light Technologies). The cuvette was irradiated across an area of 0.28 cm². The evolved headspace gas was analyzed by gas chromatography and the EQY (%) calculated via eq 3:

$$\text{EQY (\%)} = 100 \times \frac{2n_{\text{H}_2} N_{\text{A}} h c}{t_{\text{irr}} \lambda I A} \quad (3)$$

where n_{H_2} is the amount of H₂ generated (mol), N_{A} Avogadro's constant (mol⁻¹), h Planck's constant (J s), c the speed of light (m s⁻¹), t_{irr} the irradiation time (s), λ the wavelength (m), I the light intensity (W m⁻²), and A the irradiated area (m²).

Stoichiometric H₂ Conversion Calculations. Samples with 5 mg substrate in 1 M aqueous KOH (2 mL) were prepared for photocatalysis and irradiated as described above. Conversion (%) was calculated as described in eq 4:

$$\text{H}_2 \text{ conversion (\%)} = 100 \times \frac{n_{\text{H}_2, \text{exp}} n_{\text{substrate, exp}}^{-1}}{n_{\text{H}_2, \text{ideal}} n_{\text{substrate, ideal}}^{-1}} \quad (4)$$

where $n_{\text{H}_2, \text{exp}}$ is the H₂ (mol) measured in experiment, $n_{\text{substrate, exp}}$ the substrate (mol) used in experiment, and $n_{\text{H}_2, \text{ideal}} n_{\text{substrate, ideal}}^{-1}$ the ideal ratio of moles H₂ to substrate, as determined from eqs S2 and S4 in the Supporting Information.

Power Calculations. Equation 5 was used to calculate the power output from the H₂ produced.

$$\text{power (W)} = \frac{V_{\text{H}_2} n_{\text{H}_2} \rho_{\text{H}_2} u_{\text{H}_2}}{t_{\text{irr}}} \quad (5)$$

where V_{H_2} is the molar volume of H₂ at 25 °C (24.47 L mol⁻¹), n_{H_2} the moles of H₂ produced, ρ_{H_2} the density of H₂ at 25 °C (8.235 $\times 10^{-5}$ kg L⁻¹), u_{H_2} the lower heating value of H₂ (120 $\times 10^6$ J kg⁻¹), and t_{irr} the irradiation time (s).

■ ASSOCIATED CONTENT

📄 Supporting Information

The Supporting Information is available free of charge on the ACS Publications website at DOI: 10.1021/jacs.9b06872.

Chemical equations and thermodynamic calculations for the photoreforming reactions; tables containing all photocatalytic experiment data; additional X-ray photoelectron spectroscopy, powder X-ray diffraction, scanning electron microscopy, transmission electron microscopy, mass spectrometry, and nuclear magnetic reso-

nance characterization; proposed oxidation mechanism (PDF)

Data related to this publication are available at the University of Cambridge data repository: <https://doi.org/10.17863/CAM.43324>.

AUTHOR INFORMATION

Corresponding Author

*E-mail: reisner@ch.cam.ac.uk.

ORCID

Erwin Reisner: 0000-0002-7781-1616

Notes

The authors declare the following competing financial interest(s): A patent application covering carbon-based photocatalysts for photoreforming has been filed by Cambridge Enterprise (GB1808905.2).

ACKNOWLEDGMENTS

This work was supported by the Christian Doppler Research Association, Austrian Federal Ministry for Digital and Economic Affairs, National Foundation for Research, Technology and Development, OMV Group, and EPSRC (NanoDTC, EP/L015978/1 and EP/S022953/1). XPS data collection was performed at the EPSRC National Facility for XPS (HarwellXPS), operated by Cardiff University and UCL, under Contract PR 16195. We thank Dr. Heather Greer for assistance with electron microscopy, Dr. Annika Eisenschmidt for assistance with NMR, and Dr. Demetra Achilleos, Mr. Mark Bajada, Dr. Moritz Kuehnel, Dr. Nikolay Kornienko, Dr. Souvik Roy, Mr. Arjun Vijeta, and Miss Demelza Wright for useful discussions.

REFERENCES

- (1) Ellen MacArthur Foundation. The New Plastics Economy: Rethinking the Future of Plastics & Catalysing Action; 2017.
- (2) MacArthur, E. Beyond Plastic Waste. *Science* **2017**, *358*, 843.
- (3) Geyer, R.; Jambeck, J. R.; Law, K. L. Production, Use, and Fate of All Plastics Ever Made. *Sci. Adv.* **2017**, *3*, No. e1700782.
- (4) Garcia, J. M.; Robertson, M. L. The Future of Plastics Recycling. *Science* **2017**, *358*, 870–872.
- (5) Andrady, A. L. Persistence of Plastic Litter in the Oceans. In *Marine Anthropogenic Litter*; Springer International Publishing: Cham, 2015; pp 57–72.
- (6) Law, K. L.; Thompson, R. C. Microplastics in the Seas. *Science* **2014**, *345*, 144–145.
- (7) Cózar, A.; Echevarría, F.; González-Gordillo, J. I.; Irigoien, X.; Úbeda, B.; Hernández-León, S.; Palma, Á. T.; Navarro, S.; García-de-Lomas, J.; Ruiz, A.; Fernández-de-Puelles, M. L.; Duarte, C. M. Plastic Debris in the Open Ocean. *Proc. Natl. Acad. Sci. U. S. A.* **2014**, *111*, 10239–10244.
- (8) Kosuth, M.; Mason, S. A.; Wattenberg, E. V. Anthropogenic Contamination of Tap Water, Beer, and Sea Salt. *PLoS One* **2018**, *13*, No. e0194970.
- (9) Pivokonsky, M.; Cermakova, L.; Novotna, K.; Peer, P.; Cajthaml, T.; Janda, V. Occurrence of Microplastics in Raw and Treated Drinking Water. *Sci. Total Environ.* **2018**, *643*, 1644–1651.
- (10) Mason, S. A.; Welch, V. G.; Neratko, J. Synthetic Polymer Contamination in Bottled Water. *Front. Chem.* **2018**, *6*, 407.
- (11) U.S. Department of Energy. Report of the Hydrogen Production Expert Panel: A Subcommittee of the Hydrogen & Fuel Cell Technical Advisory Committee; Washington, DC, 2013.
- (12) International Energy Agency. Tracking Clean Energy Progress 2015: Energy Technology Perspectives 2015 Excerpt IEA Input to the Clean Energy Ministerial; Paris, 2015.

- (13) Spath, P. L.; Mann, M. K. Life Cycle Assessment of Hydrogen Production via Natural Gas Steam Reforming; Golden, 2001.

- (14) Chen, W.-T.; Jin, K.; Linda Wang, N.-H. Use of Supercritical Water for the Liquefaction of Polypropylene into Oil. *ACS Sustainable Chem. Eng.* **2019**, *7*, 3749–3758.

- (15) Wakerley, D. W.; Kuehnel, M. F.; Orchard, K. L.; Ly, K. H.; Rosser, T. E.; Reisner, E. Solar-Driven Reforming of Lignocellulose to H₂ with a CdS/CdO_x Photocatalyst. *Nat. Energy* **2017**, *2*, 17021.

- (16) Horikoshi, S.; Serpone, N.; Hisamatsu, Y.; Hidaka, H. Photocatalyzed Degradation of Polymers in Aqueous Semiconductor Suspensions. 3. Photooxidation of a Solid Polymer: TiO₂-Blended Poly(Vinyl Chloride) Film. *Environ. Sci. Technol.* **1998**, *32*, 4010–4016.

- (17) Ohtani, B.; Adzuma, S.; Nishimoto, S.; Kagiya, T. Photocatalytic Degradation of Polyethylene Film by Incorporated Extra-Fine Particles of Titanium Dioxide. *Polym. Degrad. Stab.* **1992**, *35*, 53–60.

- (18) Tofa, T. S.; Kunjali, K. L.; Paul, S.; Dutta, J. Visible Light Photocatalytic Degradation of Microplastic Residues with Zinc Oxide Nanorods. *Environ. Chem. Lett.* **2019**, *17*, 1341–1346.

- (19) Kuehnel, M. F.; Reisner, E. Solar Hydrogen Generation from Lignocellulose. *Angew. Chem., Int. Ed.* **2018**, *57*, 3290–3296.

- (20) Puga, A. V. Photocatalytic Production of Hydrogen from Biomass-Derived Feedstocks. *Coord. Chem. Rev.* **2016**, *315*, 1–66.

- (21) Pellegrin, Y.; Odobel, F. Sacrificial Electron Donor Reagents for Solar Fuel Production. *C. R. Chim.* **2017**, *20*, 283–295.

- (22) Kawai, T.; Sakata, T. Photocatalytic Hydrogen Production from Water by the Decomposition of Poly-Vinylchloride, Protein, Algae, Dead Insects, and Excrement. *Chem. Lett.* **1981**, *10*, 81–84.

- (23) Uekert, T.; Kuehnel, M. F.; Wakerley, D. W.; Reisner, E. Plastic Waste as a Feedstock for Solar-Driven H₂ Generation. *Energy Environ. Sci.* **2018**, *11*, 2853–2857.

- (24) Lin, L.; Yu, Z.; Wang, X. Crystalline Carbon Nitride Semiconductors for Photocatalytic Water Splitting. *Angew. Chem., Int. Ed.* **2019**, *58*, 6164–6175.

- (25) Wang, X.; Maeda, K.; Thomas, A.; Takanebe, K.; Xin, G.; Carlsson, J. M.; Domen, K.; Antonietti, M. A Metal-Free Polymeric Photocatalyst for Hydrogen Production from Water under Visible Light. *Nat. Mater.* **2009**, *8*, 76–80.

- (26) Thomas, A.; Fischer, A.; Goettmann, F.; Antonietti, M.; Müller, J.-O.; Schlögl, R.; Carlsson, J. M. Graphitic Carbon Nitride Materials: Variation of Structure and Morphology and Their Use as Metal-Free Catalysts. *J. Mater. Chem.* **2008**, *18*, 4893–4908.

- (27) Lau, V. W.; Moudrakovski, I.; Botari, T.; Weinberger, S.; Mesch, M. B.; Duppel, V.; Senker, J.; Blum, V.; Lotsch, B. V. Rational Design of Carbon Nitride Photocatalysts by Identification of Cyanamide Defects as Catalytically Relevant Sites. *Nat. Commun.* **2016**, *7*, 12165.

- (28) Meyer, A. U.; Lau, V. W.; König, B.; Lotsch, B. V. Photocatalytic Oxidation of Sulfonates to Vinyl Sulfones with Cyanamide-Functionalised Carbon Nitride. *Eur. J. Org. Chem.* **2017**, *2017*, 2179–2185.

- (29) Kasap, H.; Achilleos, D. S.; Huang, A.; Reisner, E. Photoreforming of Lignocellulose into H₂ Using Nanoengineered Carbon Nitride under Benign Conditions. *J. Am. Chem. Soc.* **2018**, *140*, 11604–11607.

- (30) Indra, A.; Acharjya, A.; Menezes, P. W.; Merschjann, C.; Hollmann, D.; Schwarze, M.; Aktas, M.; Friedrich, A.; Lochbrunner, S.; Thomas, A.; Driess, M. Boosting Visible-Light-Driven Photocatalytic Hydrogen Evolution with an Integrated Nickel Phosphide-Carbon Nitride System. *Angew. Chem., Int. Ed.* **2017**, *56*, 1653–1657.

- (31) Ye, P.; Liu, X.; Iocozzia, J.; Yuan, Y.; Gu, L.; Xu, G.; Lin, Z. A Highly Stable Non-Noble Metal Ni₃P Co-Catalyst for Increased H₂ Generation by g-C₃N₄ under Visible Light Irradiation. *J. Mater. Chem. A* **2017**, *5*, 8493–8498.

- (32) Wen, J.; Xie, J.; Shen, R.; Li, X.; Luo, X.; Zhang, H.; Zhang, A.; Bi, G. Markedly Enhanced Visible-Light Photocatalytic H₂ Generation over g-C₃N₄ Nanosheets Decorated by Robust Nickel Phosphide (Ni₁₂P₅) Cocatalysts. *Dalt. Trans.* **2017**, *46*, 1794–1802.

(33) Cao, S.; Wang, C.-J.; Fu, W.-F.; Chen, Y. Metal Phosphides as Co-Catalysts for Photocatalytic and Photoelectrocatalytic Water Splitting. *ChemSusChem* **2017**, *10*, 4306–4323.

(34) Liu, J.; Liu, Y.; Liu, N.; Han, Y.; Zhang, X.; Huang, H.; Lifshitz, Y.; Lee, S.-T.; Zhong, J.; Kang, Z. Metal-Free Efficient Photocatalyst for Stable Visible Water Splitting via a Two-Electron Pathway. *Science* **2015**, *347*, 970–974.

(35) Zeng, D.; Xu, W.; Ong, W.-J.; Xu, J.; Ren, H.; Chen, Y.; Zheng, H.; Peng, D.-L. Toward Noble-Metal-Free Visible-Light-Driven Photocatalytic Hydrogen Evolution: Monodisperse Sub-15 nm Ni₂P Nanoparticles Anchored on Porous g-C₃N₄ Nanosheets to Engineer 0D-2D Heterojunction Interfaces. *Appl. Catal., B* **2018**, *221*, 47–55.

(36) Fang, X.-X.; Ma, L.-B.; Liang, K.; Zhao, S.-J.; Jiang, Y.-F.; Ling, C.; Zhao, T.; Cheang, T.-Y.; Xu, A.-W. The Doping of Phosphorus Atoms into Graphitic Carbon Nitride for Highly Enhanced Photocatalytic Hydrogen Evolution. *J. Mater. Chem. A* **2019**, *7*, 11506–11512.

(37) Hu, S.; Li, F.; Fan, Z.; Wang, F.; Zhao, Y.; Lv, Z. Band Gap-Tunable Potassium Doped Graphitic Carbon Nitride with Enhanced Mineralization Ability. *Dalton Trans.* **2015**, *44*, 1084–1092.

(38) Lu, Z.; Li, C.; Han, J.; Wang, L.; Wang, S.; Ni, L.; Wang, Y. Construction 0D/2D Heterojunction by Highly Dispersed Ni₂P QDs Loaded on the Ultrathin g-C₃N₄ Surface towards Superhigh Photocatalytic and Photoelectric Performance. *Appl. Catal., B* **2018**, *237*, 919–926.

(39) Zhou, Z.; Wei, L.; Wang, Y.; Karahan, H. E.; Chen, Z.; Lei, Y.; Chen, X.; Zhai, S.; Liao, X.; Chen, Y. Hydrogen Evolution Reaction Activity of Nickel Phosphide Is Highly Sensitive to Electrolyte pH. *J. Mater. Chem. A* **2017**, *5*, 20390–20397.

(40) Danilovic, N.; Subbaraman, R.; Strmcnik, D.; Chang, K.-C.; Paulikas, A. P.; Stamenkovic, V. R.; Markovic, N. M. Enhancing the Alkaline Hydrogen Evolution Reaction Activity through the Bifunctionality of Ni(OH)₂/Metal Catalysts. *Angew. Chem., Int. Ed.* **2012**, *51*, 12495–12498.

(41) You, B.; Zhang, Y.; Jiao, Y.; Davey, K.; Qiao, S. Z. Negative Charging of Transition-Metal Phosphides via Strong Electronic Coupling for Destabilization of Alkaline Water. *Angew. Chem., Int. Ed.* **2019**, *58*, 11796–11800.

(42) Hou, Y.; Zhu, Y.; Xu, Y.; Wang, X. Photocatalytic Hydrogen Production over Carbon Nitride Loaded with WS₂ as Cocatalyst under Visible Light. *Appl. Catal., B* **2014**, *156–157*, 122–127.

(43) Yue, H.; Zhao, Y.; Ma, X.; Gong, J. Ethylene Glycol: Properties, Synthesis, and Applications. *Chem. Soc. Rev.* **2012**, *41*, 4218–4244.

(44) Chauhan, N. L.; Dameera, V.; Chowdhury, A.; Juvekar, V. A.; Sarkar, A. Electrochemical Oxidation of Ethylene Glycol in a Channel Flow Reactor. *Catal. Today* **2018**, *309*, 126–132.

(45) Rossiter, W. J.; Brown, P. W.; Godette, M. The Determination of Acidic Degradation Products in Aqueous Ethylene Glycol and Propylene Glycol Solutions Using Ion Chromatography. *Sol. Energy Mater.* **1983**, *9*, 267–279.

(46) Harada, H.; Sakata, T.; Ueda, T. Effect of Semiconductor on Photocatalytic Decomposition of Lactic Acid. *J. Am. Chem. Soc.* **1985**, *107*, 1773–1774.

(47) Lomate, S.; Katryniok, B.; Dumeignil, F.; Paul, S. High Yield Lactic Acid Selective Oxidation into Acetic Acid over a Mo-V-Nb Mixed Oxide Catalyst. *Sustainable Chem. Processes* **2015**, *3*, 5.

(48) Vidra, A.; Németh, A. Bio-Produced Acetic Acid: A Review. *Period. Polytech., Chem. Eng.* **2018**, *62*, 245–256.

(49) Speltini, A.; Sturini, M.; Dondi, D.; Annovazzi, E.; Maraschi, F.; Caratto, V.; Profumo, A.; Buttafava, A. Sunlight-Promoted Photocatalytic Hydrogen Gas Evolution from Water-Suspended Cellulose: A Systematic Study. *Photochem. Photobiol. Sci.* **2014**, *13*, 1410–1419.

(50) Kasap, H.; Caputo, C. A.; Martindale, B. C. M.; Godin, R.; Lau, V. W.; Lotsch, B. V.; Durrant, J. R.; Reisner, E. Solar-Driven Reduction of Aqueous Protons Coupled to Selective Alcohol Oxidation with a Carbon Nitride–Molecular Ni Catalyst System. *J. Am. Chem. Soc.* **2016**, *138*, 9183–9192.

(51) Hartline, N. L.; Bruce, N. J.; Karba, S. N.; Ruff, E. O.; Sonar, S. U.; Holden, P. A. Microfiber Masses Recovered from Conventional

Machine Washing of New or Aged Garments. *Environ. Sci. Technol.* **2016**, *50*, 11532–11538.

(52) Waste & Resources Action Programme. UK Plastics Waste-A Review of Supplies for Recycling, Global Market Demand, Future Trends and Associated Risks, 2006.

(53) Helman, C. How Much Electricity Do Your Gadgets Really Use? <https://www.forbes.com/sites/christopherhelman/2013/09/07/how-much-energy-does-your-iphone-and-other-devices-use-and-what-to-do-about-it/#79d350b42f70> (accessed June 22, 2019).

(54) Lopez, G.; Artetxe, M.; Amutio, M.; Alvarez, J.; Bilbao, J.; Olazar, M. Recent Advances in the Gasification of Waste Plastics. A Critical Overview. *Renewable Sustainable Energy Rev.* **2018**, *82*, 576–596.